ATLAS NOTE

ATLAS-CONF-2012-034

March 10, 2012

Search for long-lived charginos in anomaly-mediated supersymmetry-breaking scenarios with the ATLAS detector using 4.7 fb^{-1} data of pp collisions at $\sqrt{s}$ = 7 TeV

The ATLAS Collaboration

ATLAS-CONF-2012-034
15 March 2012

Abstract

In anomaly-mediated supersymmetry-breaking (AMSB) scenarios, the lightest chargino is predicted to have a lifetime long enough to be detected in collider experiments. This note presents an updated search for disappearing tracks resulting from decaying charginos in pp collisions at $\sqrt{s}$ = 7 TeV. The search is based on data corresponding to an integrated luminosity of 4.7 fb^{-1} collected with the ATLAS detector in 2011. The p_{T} spectrum of candidate tracks is found to be consistent with the expectation from background processes and constraints on the lifetime and the production cross section are obtained. In the minimal AMSB framework with $m_{3/2} < 32$ TeV, $m_0 < 1.5$ TeV, $\tan\beta = 5$ and $\mu > 0$, a chargino having a mass below 90 GeV and a lifetime between 0.2 ns and 90 ns is excluded at 95% confidence level. The result also gives a new constraint for a chargino having a mass up to 118 GeV.

1 Introduction

Anomaly mediation of supersymmetry-breaking (AMSB) [1, 2] models for which supergravity couplings that induce mediation are absent, and where the soft supersymmetry (SUSY) breaking is caused by loop effects, provide a calculable mass spectrum of SUSY particles. In AMSB scenarios, the lightest gaugino is the wino, and the lightest chargino ($\tilde{\chi}_1^{\pm}$) and neutralino ($\tilde{\chi}_1^0$) are the charged and neutral winos; $\tilde{\chi}_1^{\pm}$ becomes slightly heavier due to radiative corrections involving electroweak gauge bosons in the loops. Masses of charged and neutral winos are highly degenerate and this leads to a significant lifetime for the lightest chargino. Some charginos could be long-lived such that their tracks can be detected inside the tracking volume of the ATLAS detector. The chargino decays into a neutralino and a low-momentum charged pion. A track arising from such a chargino decay would be seen as a disappearing track that appears to have few associated hits in the outer region of the tracking system; therefore the analysis looks at the hits in the transition radiation tracker (TRT).

ATLAS has previously reported the initial results of the search for long-lived charginos using 1.02 fb^{-1} [3]. This note extends the analysis using the entire data sample recorded in 2011 corresponding to an integrated luminosity of 4.7 fb^{-1}.

2 The ATLAS detector

ATLAS is a multi-purpose detector [4], covering nearly the entire solid angle[1] around the collision point with layers of inner tracking devices surrounded by a superconducting solenoid providing a 2 T magnetic field, a calorimeter system and a muon spectrometer. The inner tracking detector provides tracking in the region $|\eta| < 2.5$. It consists of pixel and silicon microstrip detectors inside the TRT. The barrel TRT is divided into inner, middle and outer concentric rings of 32 modules comprising a stack in azimuthal angle; it covers the radial ranges 563 mm to 694 mm (inner), 697 mm to 860 mm (middle), 863 mm to 1066 mm (outer) and $|\eta| < 1.0$. The average numbers of SCT and TRT hits on a track going through the inner detector in the central region are about 8 and 34, respetively. The calorimeter system covers the range $|\eta| < 4.9$. The electromagnetic calorimeter is a lead/liquid-argon (LAr) detector in the barrel ($|\eta| < 1.475$) and endcap ($1.375 < |\eta| < 3.2$) regions. The hadronic calorimeters are composed of a steel and scintillator barrel ($|\eta| < 1.7$), a LAr/copper endcap ($1.5 < |\eta| < 3.2$) and a LAr forward system ($3.1 < |\eta| < 4.9$) with copper and tungsten absorbers. The muon spectrometer consists of three large superconducting toroids with 24 coils, a system of trigger chambers and precision tracking chambers which provide muon momentum measurements up to $|\eta|$ of 2.7.

3 Simulated signal samples

Simulated Monte Carlo (MC) events are used to assess the experimental sensitivity to given models. The minimal AMSB model is characterized by four parameters: the gravitino mass ($m_{3/2}$), the universal scalar mass (m_0), the ratio of Higgs vacuum expectation values at the electroweak scale ($\tan\beta$) and the sign of the higgsino mass term ($sgn(\mu)$). In this note, Isasusy from Isajet v7.80 [5] is used to calculate the SUSY mass spectrum and the decay tables. The signal

[1] ATLAS uses a right-handed coordinate system with its origin at the nominal interaction point (IP) in the centre of the detector and the z-axis coinciding with the axis of the beam pipe. The x-axis points from the IP to the centre of the LHC ring, and the y-axis points upward. Cylindrical coordinates (r, ϕ) are used in the transverse plane, ϕ being the azimuthal angle around the beam pipe. The pseudorapidity is defined in terms of the polar angle θ as $\eta = -\ln\tan(\theta/2)$.

MC samples are produced using HERWIG [6] with MRST2007 LO* [7] parton distribution functions (PDFs). These samples are produced using the parameter tune described in Ref. [8] and a detector simulation based on GEANT4 [9, 10] with multiple pp interactions per event (pile-up) to match that which was observed in data. Given the chargino mass ($m_{\tilde{\chi}_1^\pm}$) limit by the LEP2 searches [11–13] of $m_{\tilde{\chi}_1^\pm} \simeq 92$ GeV at 95% confidence level (CL), the signal models shown in Table 1 are tested. In this search, the production processes $\tilde{g}\tilde{g}$, $\tilde{q}\tilde{g}$ and $\tilde{q}\tilde{q}$ are considered. Signal cross sections are calculated at next-to-leading order in QCD corrections, including the resummation of soft gluon emission at the next-to-leading-logarithmic accuracy (NLO+NLL) [14–18] in the case of squark and gluino production with masses[2] between 200 GeV and 2 TeV[3]. An envelope of cross section predictions is defined using the 68% CL ranges of the CTEQ6.6 [19] (including the uncertainty on the strong coupling constant α_S) and MSTW2008 [20] PDF sets, together with variations of the factorisation and renormalisation scales by factors of two and one half. The nominal cross section value is taken to be the midpoint of the envelope and the uncertainty assigned is half the full width of the envelope, following closely the PDF4LHC recommendations [21]. The chargino lifetime ($\tau_{\tilde{\chi}_1^\pm}$) is set to 1 ns, the value for which this analysis has the highest sensitivity. Samples with different lifetime values for each signal model are derived by applying event weights so that the distribution of the proper lifetime follows that for a given lifetime value. The branching fraction for the decay $\tilde{\chi}_1^\pm \to \tilde{\chi}_1^0\pi^\pm$ is set to 100%.

Table 1: Parameters of AMSB signal points, chargino masses and their NLO+NLL cross sections. The parameters $\tan\beta$ and $sgn(\mu)$ are set to 5 and +1. The cross sections only include $\tilde{g}\tilde{g}$, $\tilde{q}\tilde{g}$ and $\tilde{q}\tilde{q}$ production processes.

Sample	m_0[TeV]	$m_{3/2}$[TeV]	$m_{\tilde{\chi}_1^\pm}$[GeV]	Cross section[pb]
LL01	1.5	32	90.2	6.79×10^{-2}
LL02	1.8	41	117.8	8.66×10^{-3}
LL03	2.0	51	147.7	1.16×10^{-3}

4 Data and event selection

The analysis is based on pp collision data at $\sqrt{s} = 7$ TeV recorded in 2011. The corresponding integrated luminosity is 4.7 fb^{-1} after the application of beam, detector and data quality requirements. The cascade decay of gluinos and squarks results in a final state with multiple jets and large missing transverse momentum two-vector $\vec{p}_{\mathrm{T}}^{\,\mathrm{miss}}$ (and its magnitude $E_{\mathrm{T}}^{\mathrm{miss}}$). Events are thus selected at the trigger level by requiring at least one jet with a transverse momentum (p_{T}) above 75 GeV and $E_{\mathrm{T}}^{\mathrm{miss}}$ above 55 GeV.

In order to suppress non-collision background events, additional selection criteria are applied to jets; the cuts are motivated from Ref. [22]. In addition, events are discarded if they lack a reconstructed primary vertex with at least five associated tracks with $p_{\mathrm{T}} > 0.4$ GeV. Signal candidate events are required to have no identified electron or muon candidates with $p_{\mathrm{T}} > 10$ GeV (i.e. a lepton veto), where electrons are required to pass medium identification cuts as defined in Ref. [23], and the muons are identified as in Ref. [24]. The event $E_{\mathrm{T}}^{\mathrm{miss}}$ is required to satisfy $E_{\mathrm{T}}^{\mathrm{miss}} > 130$ GeV, and requirements are imposed on the three highest p_{T} jets with

[2]The mass of the squarks are the result of averaging only the first and second generation, following the convention used in the NLO calculators.

[3]In the case of gluino-pair (associated squark-gluino) production processes, the calculations are extended until squark masses of 4.5 TeV (3.5 TeV).

$|\eta| < 2.8$. The leading jet is required to satisfy $p_{\mathrm{T}} > 130$ GeV and the second- and third-leading jets $p_{\mathrm{T}} > 60$ GeV.

The search is based on the detection of charginos decaying in the TRT. Chargino candidate tracks are expected to be high-p_{T} isolated tracks. Therefore, chargino candidate tracks are required to fulfill the following criteria:

(1) The track should have one hit in the innermost layer of the pixel detector.

(2) The track should have at least six hits in the silicon microstrip detector (SCT).

(3) The track should have $|d_0| < 1.5$ mm and $|z_0 \sin\theta| < 1.5$ mm, where d_0 and z_0 are the transverse and longitudinal impact parameters with respect to the primary vertex.

(4) The track should be isolated, i.e. there should be no other primary tracks with $p_{\mathrm{T}} > 0.5$ GeV within a cone of radius $\Delta R \equiv \sqrt{(\Delta\eta)^2 + \left(\Delta\phi\right)^2} = 0.1$.[4]

(5) A candidate track should have p_{T} above 10 GeV and have the highest p_{T} among the isolated tracks in the event.

(6) The track should point to the TRT barrel layers and not point to the inactive regions around $\eta = 0$.

(7) The number of hits in the TRT outer module associated to the track ($N_{\mathrm{TRT}}^{\mathrm{outer}}$) should be fewer than five.

The first four criteria are applied for ensuring good quality of the reconstructed primary track, and are common for all tracks. The sixth criterion is based on the extrapolated track position and works as an effective acceptance cut of $|\eta| < 0.63$. The chargino track can satisfy these conditions even when it decays in the TRT detector. Hereafter, unless explicitly stated otherwise, "high-p_{T} isolated track selection" and "disappearing track selection" indicate criteria (1)–(6) and (1)–(7), respectively.

A summary of selection requirements and data reduction is given in Table 2. The distribution of $N_{\mathrm{TRT}}^{\mathrm{outer}}$, compared to the signal and background MC expectations, is shown in Fig. 1. The background expectation, dominated by QCD multijet events, is derived from QCD multijet MC events generated with Pythia 6.4.23 [25] and normalized to the number of observed events. When charginos decay before reaching the TRT outer module, $N_{\mathrm{TRT}}^{\mathrm{outer}}$ is expected to have a value near zero; conversely, through-going tracks typically have $N_{\mathrm{TRT}}^{\mathrm{outer}} \simeq 15$. The sample of selected tracks with the high-p_{T} isolated track selection criteria is dominated by through-going tracks with $N_{\mathrm{TRT}}^{\mathrm{outer}} \simeq 15$. In events in the signal sample, there is also a significant contribution of non-chargino tracks and the purity of chargino tracks, defined as the fraction of candidate tracks matched to generated charginos, is 66.8%; the peak at $N_{\mathrm{TRT}}^{\mathrm{outer}} \simeq 15$ is also predicted due to non-chargino tracks and late decaying charginos. Criterion (7) removes the vast majority of these tracks: although it reduces the signal efficiency, it strongly enhances the expected signal to background ratio. These criteria select charginos decaying in the inner and middle TRT modules ($r < 863$mm) effectively. The purity of chargino tracks is above 94% in signal events; a small contribution of non-chargino tracks still remains, however, they make up the population at $p_{\mathrm{T}} \simeq 10$ GeV and can be rejected when determining the signal yield (Section 7).

[4] A cone of radius 0.05 was previously used for the track isolation [3] while the current analysis uses a cone of radius 0.1. A tighter requirement of track isolation removes background tracks while retaining a high signal selection efficiency, resulting in an enhanced signal to background ratio.

Requirement	Observed events	Signal efficiency (purity) [%]		
		LL01	LL02	LL03
Trigger selection and non-collision rejection	7141026	87.3	89.1	90.1
Lepton veto	6644394	72.8	72.5	72.6
$E_{\mathrm{T}}^{\mathrm{miss}} > 130$ GeV	321412	66.5	68.2	69.6
Jet requirements	73433	64.9	67.4	69.0
High-p_{T} isolated track selection	8458	24.8 (67.6)	26.2 (66.8)	27.2 (66.7)
Disappearing track selection	304	6.1 (94.6)	6.6 (94.5)	7.3 (94.7)

Table 2: Summary of selection cuts, the data reduction and the selection efficiencies for the AMSB signals. The purities of chargino tracks, i.e. the fraction of selected tracks in signal events originating from charginos, are also shown in parentheses.

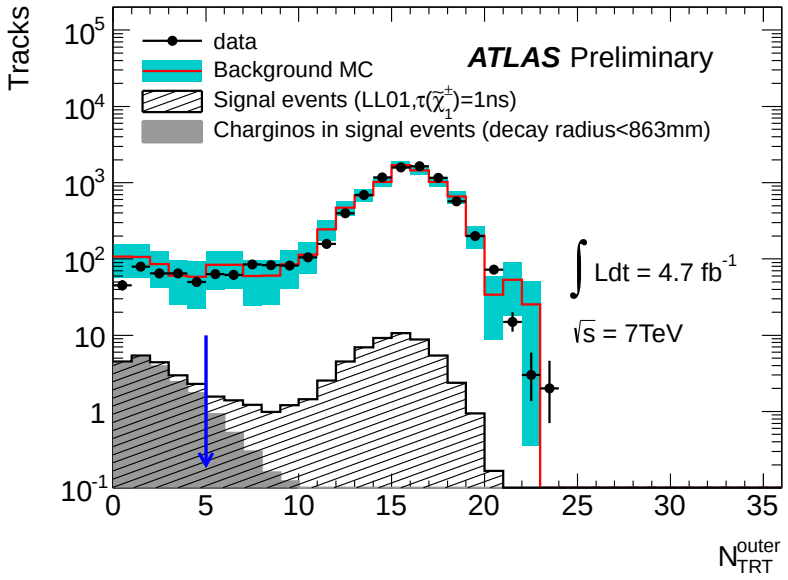

Figure 1: The $N_{\mathrm{TRT}}^{\mathrm{outer}}$ distributions for data and signal events (LL01, $\tau_{\tilde{\chi}_1^{\pm}} = 1$ ns) shown by the hatched histogram with the high-p_{T} isolated track selection. In the signal events, the contribution of tracks matched to generated charginos that decay before reaching the TRT outer module ($r < 863$ mm) is indicated by the filled histogram. For these tracks, $N_{\mathrm{TRT}}^{\mathrm{outer}}$ is expected to have a value near zero; conversely, charged particles traversing the TRT typically have $N_{\mathrm{TRT}}^{\mathrm{outer}} \simeq 15$. The selection boundary is indicated by the arrow. The expectation from QCD multijet background MC events, normalized to the number of observed events, is also shown.

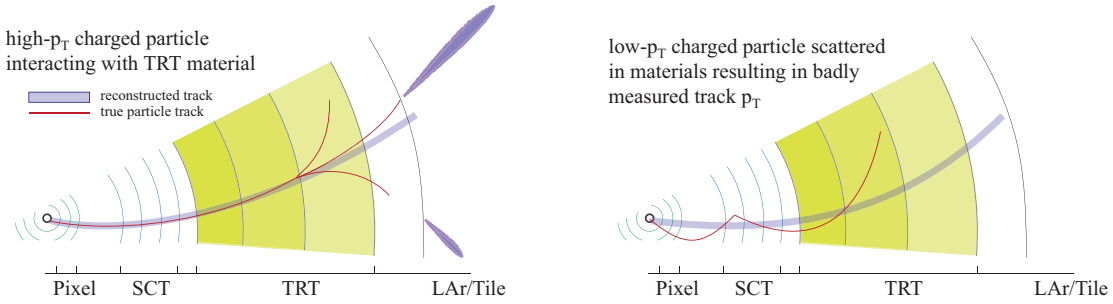

(a) High-p_T interacting hadron track (b) Bad track

Figure 2: Illustration of background tracks.

5 Background estimation

With all the selection criteria described in the previous section, there are two main background sources that contribute to the events containing such high-p_T disappearing tracks:

1. Interacting hadron track
   When charged hadrons interact with the material of the TRT detector, the tracks fulfill the track selection requirements except that they give smaller numbers of $N_{\mathrm{TRT}}^{\mathrm{outer}}$. These tracks dominate the background and predominantly originate from charged hadrons in jets and hadronic τ decays.

2. Badly reconstructed track
   Low-p_T charged particles could be badly measured in p_T due to scattering in the inner detector material. These tracks are most likely seeded from low-p_T charged particles due to a wrong combination of SCT space-points, therefore, they have small numbers of $N_{\mathrm{TRT}}^{\mathrm{outer}}$.

The two categories are labelled as "high-p_T interacting hadron track" and "bad track" backgrounds, respectively. Other contributions such as electrons having low p_T, classified as candidate tracks due to bremsstrahlung, are found to be small, and are neglected.

A fully data-driven technique is used to estimate the background track p_T spectrum, which uses control samples enriched in the two background categories. Fig. 2(a) and Fig. 2(b) show schematically the origins of background tracks. The control samples are selected to be orthogonal to the signal search samples using the number of pixel hits and $N_{\mathrm{TRT}}^{\mathrm{outer}}$. In addition, a requirement on calorimeter activity $C \equiv \sum_{\Delta R<0.1} E_{\mathrm{T}}^{\mathrm{clus}}/p_{\mathrm{T}}^{\mathrm{track}}$ (the sum of calorimeter cluster transverse energies in a cone of $\Delta R = 0.1$ around the track divided by the p_T of the track) is used to further purify the samples and make the selections for each background orthogonal to the other.

High-p_T interacting hadron tracks The main contribution to the high-p_T interacting hadron background originates from charged hadrons in jets and τ hadronic decays. In the p_T range above 10 GeV, where inelastic interactions dominate, the interaction rate has nearly no p_T-dependence [26]. Therefore, the p_T spectrum of interacting hadron tracks is obtained from that of non-interacting hadron tracks. By adopting the same kinematic selection criteria as those for

the signal and ensuring penetration through the TRT detector by requiring $N_{\mathrm{TRT}}^{\mathrm{outer}} > 10$, a pure sample of high-$p_{\mathrm{T}}$ non-interacting hadron tracks is obtained. Non-interacting hadron tracks are expected to have a matching energy deposit in the calorimeter. The contamination from bad tracks and any chargino signal is then removed by requiring $C > 0.3$.

Bad tracks A sample with an enhanced bad track contribution is obtained with the same track quality requirements as for the chargino track, but requiring $E_{\mathrm{T}}^{\mathrm{miss}} < 100$ GeV. In addition, the number of pixel hits associated to the track is required to be zero, and $C < 0.3$ in order to reject possible contributions from high-p_{T} interacting hadron tracks and to enhance the purity of bad tracks. The requirement on the number of pixel hits has a negligible impact on the shape of the reconstructed p_{T} spectrum.

The high-p_{T} interacting hadron tracks show a steeply falling p_{T} spectrum with a high-p_{T} tail. In order to develop a data-driven p_{T} spectrum of the high-p_{T} hadron background tracks, an ansatz functional form

$$\frac{(1+x)^{a_0}}{x^{a_1+a_2\ln(x)}} \tag{1}$$

is used, where $x \equiv p_{\mathrm{T}}^{\mathrm{track}}$ and a_i $(i = 0, 1, 2)$ are fit parameters. This functional form is fitted to the p_{T} spectrum of the control samples of high-p_{T} non-interacting hadron tracks. The bad tracks could have anomalously high values of p_{T}. Therefore, for the bad track background shape, a flat term representing the high-p_{T} tail is added to Eq. 1. Extra Pixel and SCT hits due to pile-up could alter the p_{T} spectrum of bad tracks, however, no significant differences depending on the number of reconstructed primary vertices are found. The p_{T} distributions of the signal, interacting hadron track and bad track backgrounds are shown in Fig. 3.

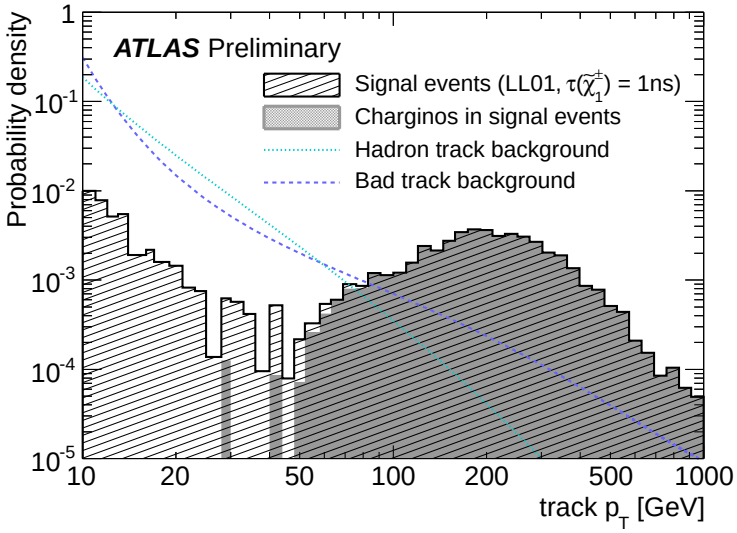

Figure 3: The p_{T} distribution of the signal (LL01, $\tau_{\tilde{\chi}_1^\pm} = 1$ ns) shown by the hatched histogram together with the background components, fitted from control samples in data. In the signal events, the contribution of tracks matched to generated charginos is indicated by the filled histogram. A small contribution of non-chargino tracks (about 5%, predominantly originating from high-p_{T} interacting hadrons) in the signal events is expected in the region $p_{\mathrm{T}} < 50$ GeV.

6 Systematic uncertainties

The following sources of systematic uncertainty on the signal normalisation have been considered: the theoretical cross section, the jet energy scale (JES), the track reconstruction efficiency, the integrated luminosity, the pile-up modeling and the trigger efficiency.

Theoretical uncertainties on the signal cross section are evaluated by computing the changes in the cross section when the renormalisation and factorisation scales, the choice of PDFs and α_S are varied, as described in Section 3. A total uncertainty of ±27% is assigned on the theoretical cross section. The uncertainty of the overall normalisation arising from JES in multi-jet environments is assessed according to Ref. [27]. The uncertainty on $E_{\mathrm{T}}^{\mathrm{miss}}$ due to JES is also taken into account in a coherent way; the resulting uncertainty is estimated to be ±3%. The modeling of the inner detector material alters the track reconstruction efficiency and affects the signal selection efficiency. An uncertainty of ±2% is applied to the tracking efficiency due to limited knowledge of material in the inner detector [28]. The uncertainty on the integrated luminosity is estimated to be ±3.9%, as extrapolated from Ref. [29, 30]. The uncertainty originating from the pile-up modeling in the simulation is evaluated by taking the difference in the acceptance between the nominal sample and one where the pile-up contribution is reweighted based on the average number of pile-up interactions; an uncertainty of ±0.5% is assigned. By accounting for the difference between the measured trigger efficiency and the MC expectation as a function of $E_{\mathrm{T}}^{\mathrm{miss}}$, an uncertainty of ±2% is applied. In total, an uncertainty of ±28% is found for the signal normalisation.

The uncertainties of the background p_{T}-shapes are taken into account using the covariance matrices obtained from the fit of the background control samples. The resulting uncertainty on the background estimate is small.

7 Results

The statistical analysis employs a likelihood function for the samples of observed events using the track p_{T}. The full shape of the distributions for $p_{\mathrm{T}} > 10$ GeV is fitted with the two background contributions, and a signal contribution is also included in the fit for $p_{\mathrm{T}} > 50$ GeV. A contribution below 50 GeV in signal events is neglected in order to ensure a p_{T} spectrum consisting of pure chargino tracks. The overall normalisation of the signal and the parameters describing the background track p_{T} shapes are also fitted with constraints; they are treated with a normal distribution and multivariate normal distributions with covariance matrices obtained by the fit of the background control samples, respectively. Fig. 4 shows the best-fit shape of the 'signal + background' model for the sample signal point LL01 with $\tau_{\tilde{\chi}_1^\pm} = 1$ ns. The best fit is consistent with zero signal events. The p-value for the consistency of the observed data with the background-only hypothesis is calculated to be 0.5, showing that the observed track p_{T} spectrum is in agreement with the background expectation. The result also indicates that interacting hadron tracks are the dominant background, which is consistent with MC predictions.

The upper limit on the production cross section for a given model at 95% CL is then set by a point where the CL of the 'signal + background' hypothesis, based on the profile likelihood ratio [31] and the *CLs* method [32], falls below 5% when scanning CL along various values of signal strength. Fig. 5 and 6 show the observed limits of the signal cross section for the LL01 and LL02 models at the 95% CL as a function of the lifetime of the chargino. Charginos with a mass of 90.2 GeV and lifetimes in the range $0.2 < \tau_{\tilde{\chi}_1^\pm} < 90$ ns are excluded. Charginos with a mass of 117.8 GeV and lifetimes in the range $1 < \tau_{\tilde{\chi}_1^\pm} < 2$ ns are also excluded. A constraint on the chargino mass and lifetime is also set for models with $m_{3/2} < 32$ TeV, $m_0 < 1.5$ TeV, $\tan\beta = 5$ and

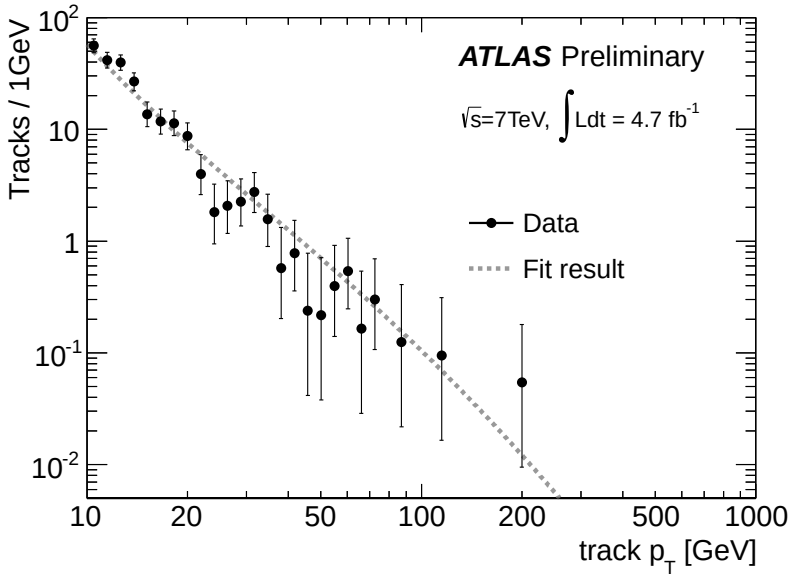

Figure 4: The p_{T} distribution of candidate tracks with the best-fit shape of the 'signal + background' model. The signal point of LL01 and $\tau_{\tilde{\chi}_1^\pm} = 1$ ns are used, but the best-fit signal contribution is found to be zero.

$\mu > 0$, as shown in Fig. 7. Using the given models, 95% CL upper limits of the signal strength (μ_{s}^{95}, defined as the ratio of signal cross section to the model expectation) for three masses of 90.2, 117.8 and 147.7 GeV are obtained at each value of lifetime. By linear interpolation with these limits, the constraint on the mass is then set by the point where μ_{s}^{95} becomes less than one. Previous results from LEP2 [11–13] constrained $m_{\tilde{\chi}_1^\pm} > 92$ GeV at 95% CL. This result improves on these constraints such that $m_{\tilde{\chi}_1^\pm} > 118$ GeV at 95% CL for $\tau_{\tilde{\chi}_1^\pm}$ close to 1 ns.

Moreover, model-independent upper limits are set on the cross section times the acceptance for non-SM processes with final state satisfying the kinematic and track selection criteria. Fig. 8 shows upper limits on a cross section times acceptance from a counting of candidate tracks for $p_{\mathrm{T}} > p_{\mathrm{T}}^0$ as a function of p_{T}^0; the background estimate is derived from the background-only fit in the region $10 < p_{\mathrm{T}} \leq 50$ GeV. A limit of 0.94×10^{-3} pb (95% CL) is obtained for disappearing tracks having p_{T} larger than 100 GeV.

8 Conclusion

The results of a search for long-lived charginos in pp collisions with the ATLAS detector using 4.7 fb^{-1} of data have been presented in the context of AMSB scenarios. The analysis uses a signature of high-p_{T} isolated tracks with few associated hits in the outer part of the ATLAS tracking system. The p_{T} spectrum of observed candidate tracks is found to be consistent with the expectation from SM background processes. Constraints on the AMSB chargino mass and lifetime are set: a chargino having a mass below 90 (118) GeV and 0.2 (1) $< \tau_{\tilde{\chi}_1^\pm} <$ 90 (2) ns is excluded at 95% CL. The result also gives a new constraint for a chargino having a mass up to 118 GeV.

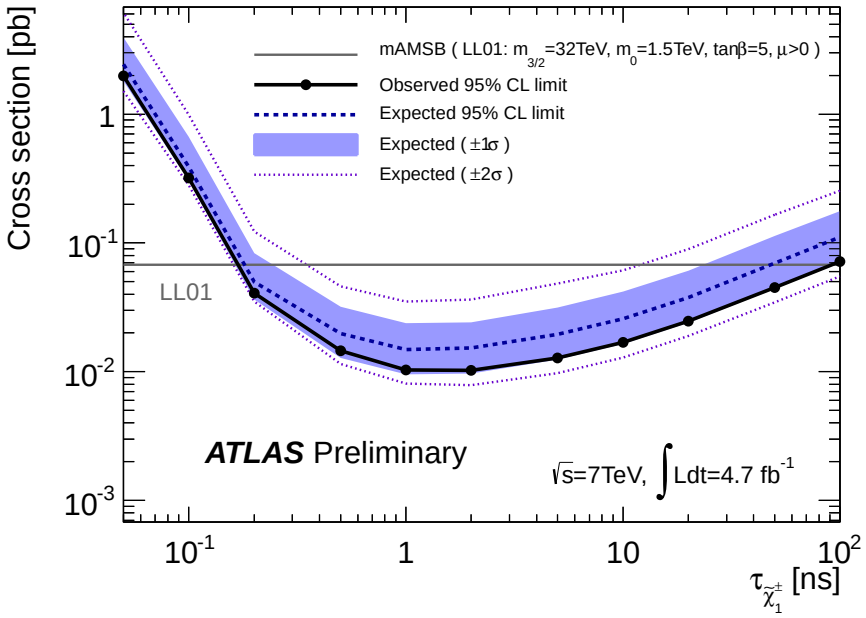

Figure 5: The observed and expected upper limits on the signal cross section as a function of chargino lifetime at 95% CL for $m_{\tilde{\chi}_1^\pm} = 90.2$ GeV. The band and dotted line indicate the range where the limit is expected to lie, assuming no signal.

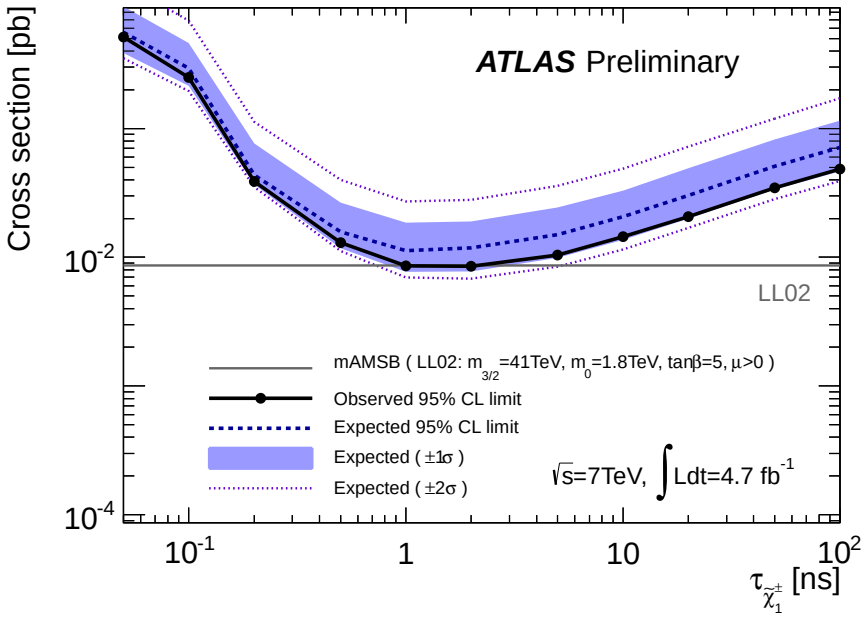

Figure 6: The observed and expected upper limits on the cross section as a function of the chargino lifetime at 95% CL for $m_{\tilde{\chi}_1^\pm} = 117.8$ GeV.

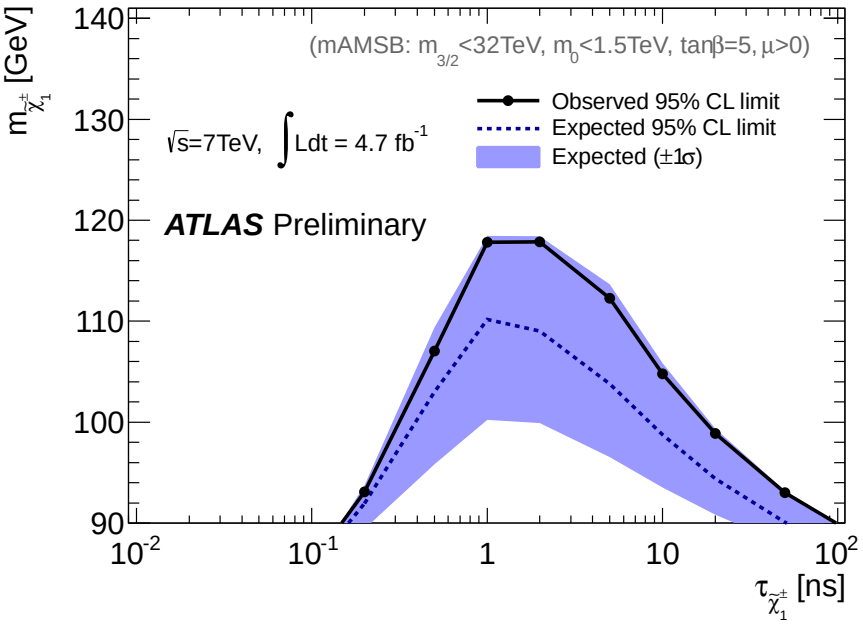

Figure 7: The constraint on $m_{\tilde{\chi}_1^\pm}$ and $\tau_{\tilde{\chi}_1^\pm}$. The observed bound at 95% CL and the expected bound with an integrated luminosity of 4.7 fb^{-1} are shown.

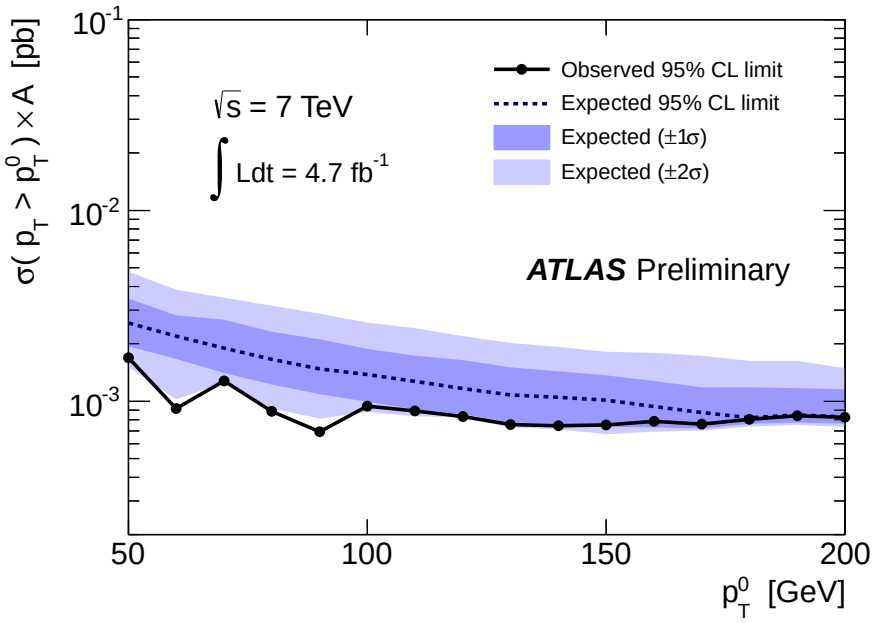

Figure 8: Model-independent upper limits on the cross section times the acceptance for an non-SM physics production with an isolated disappearing track with $p_{\mathrm{T}} > p_{\mathrm{T}}^0$ as a function of p_{T}^0. The observed bound at 95% CL and the expected bound with an integrated luminosity of 4.7 fb^{-1} are shown. The background estimate is derived from the background-only fit in the region $10 < p_{\mathrm{T}} \leq 50$ GeV.

References

[1] G. F. Giudice, M. A. Luty, H. Murayama, and R. Rattazzi, *Gaugino Mass without Singlets*, JHEP **12** (1998) 027, arXiv:hep-ph/9810442.

[2] L. Randall and R. Sundrum, *Out of this world supersymmetry breaking*, Nucl. Phys. **B557** (1999) 79–118, arXiv:hep-th/9810155.

[3] ATLAS Collaboration, *Search for anomaly-mediated supersymmetry breaking with the ATLAS detector based on a disappearing-track signature in pp collisions at* $\sqrt{s}$ *= 7 TeV*, arXiv:1202.4847 [hep-ex]. submitted to Eur. Phys. J. C.

[4] ATLAS Collaboration, *The ATLAS Experiment at the CERN Large Hadron Collider*, JINST **3** (2008) S08003.

[5] F. E. Paige, S. D. Protopopescu, H. Baer, and X. Tata, *ISAJET 7.69: A Monte Carlo event generator for pp, anti-p p, and e+e- reactions*, arXiv:hep-ph/0312045.

[6] G. Corcella et al., *HERWIG 6.5 release note*, arXiv:hep-ph/0210213.

[7] A. Sherstnev and R. S. Thorne, *Parton Distributions for LO Generators*, Eur. Phys. J. **C55** (2008) 553–575, arXiv:0711.2473 [hep-ph].

[8] ATLAS Collaboration, *Charged particle multiplicities in p p interactions at* $\sqrt{s}$ *= 0.9 and 7 TeV in a diffractive limited phase-space measured with the ATLAS detector at the LHC and new PYTHIA6 tune*, ATLAS-CONF-2010-031, 2010.

[9] GEANT4 Collaboration, S. Agostinelli et al., *GEANT4: A simulation toolkit*, Nucl. Instrum. Meth. **A506** (2003) 250–303.

[10] ATLAS Collaboration, *The ATLAS Simulation Infrastructure*, Eur. Phys. J. **C70** (2010) 823–874, arXiv:1005.4568 [physics.ins-det].

[11] ALEPH Collaboration, A. Heister et al., *Search for charginos nearly mass degenerate with the lightest neutralino in e+ e- collisions at center-of-mass energies up to 209-GeV*, Phys.Lett. **B533** (2002) 223–236, arXiv:hep-ex/0203020.

[12] OPAL Collaboration, *Search for nearly mass degenerate charginos and neutralinos at LEP*, Eur. Phys. J. **C29** (2003) 479–489, arXiv:hep-ex/0210043.

[13] DELPHI Collaboration, *Search for SUSY in the AMSB scenario with the DELPHI detector*, Eur. Phys. J. **C34** (2004) 145–156, arXiv:hep-ex/0403047.

[14] W. Beenakker, R. Hopker, M. Spira, and P. Zerwas, *Squark and gluino production at hadron colliders*, Nucl. Phys. **B492** (1997) 51–103, arXiv:hep-ph/9610490 [hep-ph].

[15] A. Kulesza and L. Motyka, *Threshold resummation for squark-antisquark and gluino-pair production at the LHC*, Phys. Rev. Lett. **102** (2009) 111802, arXiv:0807.2405 [hep-ph].

[16] A. Kulesza and L. Motyka, *Soft gluon resummation for the production of gluino-gluino and squark-antisquark pairs at the LHC*, Phys. Rev. **D80** (2009) 095004, arXiv:0905.4749 [hep-ph].

[17] W. Beenakker, S. Brensing, M. Kramer, A. Kulesza, E. Laenen, et al., *Soft-gluon resummation for squark and gluino hadroproduction*, JHEP **0912** (2009) 041, arXiv:0909.4418 [hep-ph].

[18] W. Beenakker, S. Brensing, M. Kramer, A. Kulesza, E. Laenen, et al., *Squark and gluino hadroproduction*, Int.J.Mod.Phys. **A26** (2011) 2637–2664, arXiv:1105.1110 [hep-ph].

[19] P. M. Nadolsky et al., *Implications of CTEQ global analysis for collider observables*, Phys. Rev. **D78** (2008) 013004, arXiv:0802.0007 [hep-ph].

[20] A. Martin, W. Stirling, R. Thorne, and G. Watt, *Parton distributions for the LHC*, Eur. Phys. J. **C63** (2009) 189–285, arXiv:0901.0002 [hep-ph].

[21] M. Botje, J. Butterworth, A. Cooper-Sarkar, A. de Roeck, J. Feltesse, et al., *The PDF4LHC Working Group Interim Recommendations*, arXiv:1101.0538 [hep-ph].

[22] ATLAS Collaboration, *Data-Quality Requirements and Event Cleaning for Jets and Missing Transverse Energy Reconstruction with the ATLAS Detector in Proton-Proton Collisions at a Center-of-Mass Energy of sqrts = 7 TeV*, ATLAS-CONF-2010-038, 2010.

[23] ATLAS Collaboration, *Measurement of the $W \to l\nu$ and $Z/\gamma^* \to ll$ production cross sections in proton-proton collisions at $\sqrt{s} = 7$ TeV with the ATLAS detector*, JHEP **1012** (2010) 060, arXiv:1010.2130 [hep-ex].

[24] ATLAS Collaboration, *Measurement of the Transverse Momentum Distribution of W Bosons in pp Collisions at $\sqrt{s} = 7$ TeV with the ATLAS Detector*, Phys. Rev. **D85** (2012) 012005, arXiv:1108.6308 [hep-ex].

[25] T. Sjostrand, S. Mrenna, and P. Z. Skands, *PYTHIA 6.4 Physics and Manual*, JHEP **0605** (2006) 026, arXiv:hep-ph/0603175.

[26] K. Nakamura et al., *Review of particle physics*, J.Phys. **G37** (2010) 075021. corresponding data may be found at pages 398-399.

[27] ATLAS Collaboration, *Jet energy measurement with the ATLAS detector in proton-proton collisions at $\sqrt{s} = 7$ TeV*, arXiv:1112.6426 [hep-ex]. submitted to Eur. Phys. J. C.

[28] ATLAS Collaboration, *Measurements of underlying-event properties using neutral and charged particles in pp collisions at 900 GeV and 7 TeV with the ATLAS detector at the LHC*, Eur. Phys. J. **C71** (2011) 1636, arXiv:1103.1816 [hep-ex].

[29] ATLAS Collaboration, *Luminosity Determination in pp Collisions at $\sqrt{s} = 7$ TeV Using the ATLAS Detector at the LHC*, Eur. Phys. J. **C71** (2011) 1630, arXiv:1101.2185 [hep-ex].

[30] ATLAS Collaboration, *Luminosity Determination in pp Collisions at $\sqrt{s} = 7$ TeV using the ATLAS Detector in 2011*, ATLAS-CONF-2011-116, 2011.

[31] G. Cowan, K. Cranmer, E. Gross, and O. Vitells, *Asymptotic formulae for likelihood-based tests of new physics*, Eur. Phys. J. **C71** (2011) 1554, arXiv:1007.1727 [physics.data-an].

[32] A. L. Read, *Presentation of search results: The CL(s) technique*, J. Phys. **G28** (2002) 2693–2704.